LASER
& PHOTONICS
REVIEWS

Laser Photonics Rev. **11,** No. 1, 1600257 (2017) / **DOI** 10.1002/lpor.201600257

LETTER
ARTICLE

Abstract A high-performance UV photodetector (PD) based on a p-Se/n-ZnO hybrid structure with large area (more than 1×1 cm) is presented in this study. The device is theoretically equivalent to a parallel-connection circuit for its special structure and shows multifunction at different voltage bias, which means the output signal can be tailored by an applied voltage. The Se/ZnO PD shows binary response (positive and negative current output under on/off periodical light illumination) under small reverse bias (–0.05 V and –0.1 V) which efficiently reduces the negative effect of noise signal in weak-signal detection applications. At zero bias, with the aid of a p-n heterojunction, a high on/off ratio of nearly 10^4 is achieved by this device at zero set bias under 370 nm (~0.85 mW cm^{-2}) illumination and this on/off ratio can be achieved in 0.5 s. The device also shows a fast speed with rise time of 0.69 ms and decay time of 13.5 ms measured by a pulse laser, much faster than that of a pure ZnO film. The Se/ZnO PD in this research provides a new pathway to fabricate multifunctional high-speed, high signal-to-noise ratio, high detectivity and high selectivity UV photodetectors.

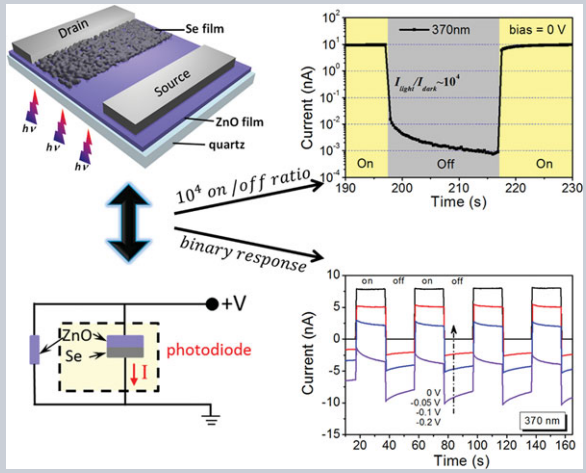

Binary response Se/ZnO p-n heterojunction UV photodetector with high on/off ratio and fast speed

Kai Hu, Feng Teng, Lingxia Zheng, Pingping Yu, Zhiming Zhang, Hongyu Chen, and Xiaosheng Fang*

1. Introduction

UV photodetectors (PDs) are vital to many commercial and scientific applications including optical communication, flame sensing, biological and chemical analysis, satellite launch and astronomical studies [1]. It is commonly accepted that an outstanding PD should satisfy "5S" requirements: high sensitivity, high signal-to-noise ratio, high spectral selectivity, high speed, and high stability [2]. ZnO is a widely studied UV detection material for many of its merits. The bandgap of ZnO is about 3.37 eV, which indicates its excellent UV selectivity. Many ZnO PDs with various nanostructures, such as thin films [3], nanowires (array) [4, 5], nanobelts [6], nanorods [7], and nanoparticles [8, 9] are reported to demonstrate high UV sensitivity and stability. However, large surface-to-volume ratio of nanostructures usually allows abundant O_2 adsorption [3], leading to long rise and decay time, usually of the order of seconds [10]. In addition to low speed, a constant bias voltage is needed for ZnO nanostructured photoconductive type or metal–semiconductor–metal (MSM) PDs to separate photogenerated electron–hole pairs [11], which usually result in a relatively low signal-to-noise ratio (high dark current) and energy consumption. Many recent studies have focused on specially designed ZnO nanostructures to improve the signal-to-noise ratio and have achieved significant progress. For example, the ultraporous electron-depleted ZnO nanoparticle networks [12–15] achieve ultrahigh photo-to-dark ratio of 10^5–10^7 and graphdiyne–ZnO nanocomposites based PDs [3] also achieves photo-to-dark ratios of ~10^6. Although these new ideas greatly improves the signal-to-noise ratio, a constant-voltage bias, albeit small, is needed for the operation of these PDs, not to mention their relative long response time, up to several seconds.

To further reduce or even eliminate the energy consumption of PDs, many efforts have been paid on zero-bias operational or self-powered PDs that harvest energy from detected light [16, 17]. The self-powered PDs are usually based on the photovoltaic effect via Schottky junctions [16, 18] or p-n junctions [17, 19]. Although previously reported ZnO self-powered PDs based on Schottky junctions are able to work at zero bias, the oxygen photodesorb/readsorbs process still hinders the speed of ZnO PDs [8]. Comparing with a Schottky junction, a p-n junction might be the perfect candidate to achieve self-powered detection and high speed. The built-in electric field can effectively separate photogenerated electrons and holes, which means an external bias voltage is not needed. This will greatly reduce the energy consumption of every single photodetector. In spite of the photovoltaic effect, previous studies also showed that ZnO p-n photodiodes have the advantage of short rise and decay time and show no oxygen

Department of Materials Science, Fudan University, 220 Handan Road, Shanghai 200433, China
*Corresponding author: e-mail: xshfang@fudan.edu.cn

dependence on speed [20]. Usually, a high-speed p-type semiconductor is preferred to achieve fast response of the whole ZnO-based p-n junction photodiode.

Selenium (Se), as an intrinsic p-type elemental semiconductor material [21, 22], is a prospective candidate to improve the performance of ZnO-based PDs. Se has attracted many studies in recent years for many novel physical properties, such as low melting point (~220°C), high conductivity ($\sim 8\times10^4$ S cm^{-1}), high intrinsic carrier concentration ($\sim 9.35\times10^{16}$ cm^{-3}) [23, 24]. Recently, researchers have paid much attention to selenium-based photodetectors via various nanostructures, such as thin films, nanowires, nanobelts, nanotubes, etc. [25, 26]. Previous reports on Se-based photodetectors reveal that Se PDs exhibit intrinsic fast response speed of several microseconds without any treatment [24, 25, 27]. For example, photodetector based on a single Se nanobelt has a rise time of 0.57 ms and a decay time of 2.65 ms. [24]. Therefore, Se is a promising p-type material to construct p-n junctions with ZnO to achieve self-powered and high-speed photodetectors.

In this work, we fabricate a zero-bias operational p-n heterojunction photodetector based on an n-type ZnO nanoparticle film and a p-type Se microcrystals film with a simple combination of spin coating and vapor phase deposition methods. The device shows multifunctional response at different voltage biases. At low reverse bias (–0.05 V and –0.1 V), the photodetector shows a rapid binary response with current changing between negative and positive upon on/off light irradiation. The binary response phenomenon is a novel and effective method to produce bidirectional output current directly. This interesting phenomenon might be potentially used for binary light communication and other applications related to weak-signal detection, which is well explained by the parallel connection of ZnO and Se/ZnO photodetectors originating from the special pattern of indium electrodes of the device. At zero applied bias, the device demonstrates both high speed and UV selective photoresponse (a UV-vis rejection ratio of >10) of the ZnO film. Moreover, the photocurrent reaches 10 nA at 370-nm UV radiation with a low power density of 0.85 mW cm^{-2} and the dark current is very low, about 1 pA. The on-off ratio of this device reaches 10^4 under the wavelength of 370 nm within 0.5 s, measured by a Keithley 4200-SCS semiconductor characterization system with a quasisteady-state UV light source. The speed of the device is very fast with a rise time (from 10% to 90%) of 0.69 ms and a decay time (from 90% to 10%) of 13.5 ms measured by a pulse laser with pulse duration: 3–5 ns. Furthermore, the responsivity of the device is calculated as 2.65 mA W^{-1} at zero bias and 60 mA W^{-1} at 5 V bias upon 370-nm UV illumination. Therefore, the Se/ZnO p-n heterojunction device is a promising candidate for a high-performance multifunctional UV photodetector.

2. Experimental section

ZnO film preparation: zinc acetate (1g) and polyvi nylpyrrolidone (PVP, 1 g) were added into 10 mL of pure DI water. The solution was stirred for 2 h while 0.1 ml acetic acid was added into the solution slowly. Then, a thin and transparent film was prepared by spin coating the mixed solution on cleaned quartz substrates. The substrates are then annealed for 150 min at 550°C to remove the PVP and crystallize ZnO.

Se/ZnO hybrid film preparation: a Se microcrystal film is then grown on the as-fabricated ZnO film that is half-covered. The synthesis of the Se film is carried out in a horizontal tube furnace via vapor transport and deposition process. The Se source (> 99.95%, Meixing chemical co., LTD, Shanghai) was in the center of the furnace and the quartz substrates with the thin ZnO film was placed 38 cm downstream from the center vertically. Before heating, ultrapure nitrogen was flushed at a rate of 400 sccm for nearly 30 min to remove residual air. Then, the center temperature of tube furnace is raised to 300°C in 55 min and maintain at 300°C for 600 min with a constant nitrogen flow of 300 sccm. The furnace is then cooled to room temperature naturally. Two indium electrodes are patterned on the ZnO and Se film respectively as depicted in Fig. 2a.

Material characterization: The morphology of the as-synthesized Se/ZnO hybrid structure was characterized by a field-emission scanning electron microscopy (FESEM, Zeiss Sigma) and the phase of the material is further identified by X-ray diffraction (XRD, Bruker D8-A25) using CuK_α radiation ($\lambda = 0.15406$ nm) in the 2θ range from 20° to 60°. The optical properties of elemental Se are characterized using a UV-visible spectrophotometer (Hitachi U-3900H).

Photoelectric measurements: The photoelectric properties (*I–V* and *I–t* characteristics) and spectral photoresponses of the device are characterized by semiconductor characterization system (Keithley 4200-SCS), a 24-W Xe lamp (POWERMAX II P21NRX3) and monochromators. The time-resolved responses of the device are measured with YAG:Nd laser (Continuum Electro-Optics, MINILITE II, 355 nm, pulse duration: 3–5 ns),oscilloscope (Tektronix MSO/DPO5000) and a 1-GΩ resistor.

3. Results and discussion

The morphology of the as-fabricated Se/ZnO heterojunction PD is characterized by field-emission scanning electron microscopy (FESEM) as depicted in Fig. 1. Figure 1a shows the surface of Se/ZnO PD in large area where half of the ZnO film is covered by a Se film (dark color) prepared by a vapor deposition method. The enlarged image of ZnO nanoparticle film in Fig. 1b demonstrates that the thin film of ZnO consists of small nanoparticles with good uniformity. The sizes of the nanoparticles are mainly concentrated within 20–90 nm with a mean diameter of 47 nm as depicted in the size distribution of the ZnO nanoparticles given in Fig. S1. The SEM images of deposited Se microcrystals on ZnO film are presented in Fig. 1c and 1d with different magnifications. It is obvious that Se microcrystals cover the ZnO film with good uniformity in large area, as shown in Fig. 1c. More details of these Se microcrystals

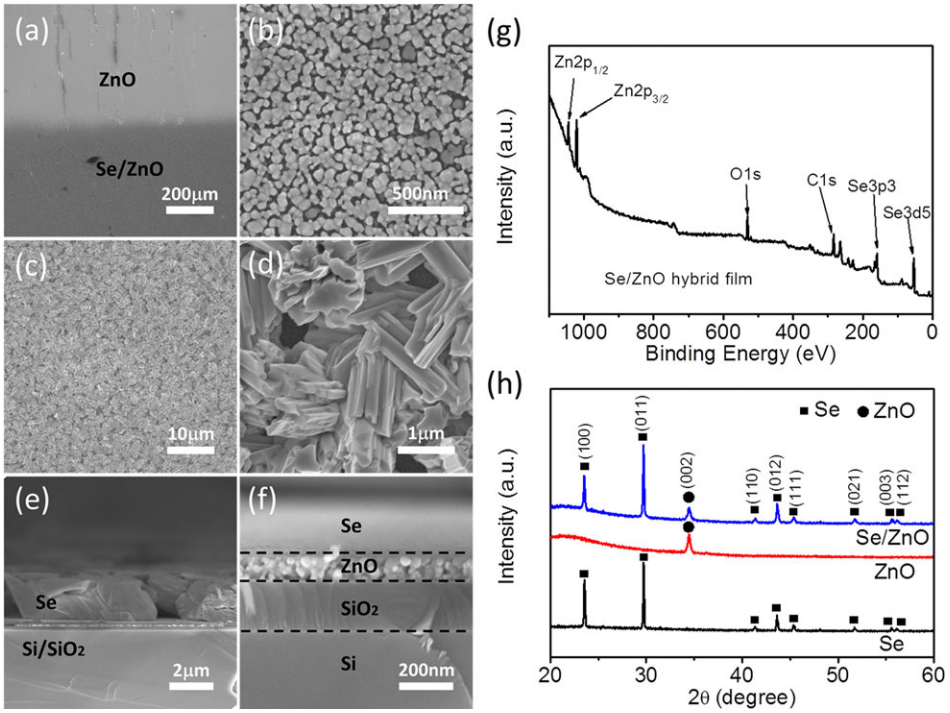

Figure 1 Plane-view SEM image of (a) Se/ZnO hybrid structure in large area; (b) ZnO nanoparticle film; (c) Se/ZnO hybrid film; (d) Magnified image of Se/ZnO hybrid film in (c); (e, f) Cross-sectional SEM images of Se/ZnO hybrid structure on Si/SiO_2 substrate at different magnifications. (g) XPS analysis of Se/ZnO hybrid film. (h) XRD patterns of Se, ZnO and Se/ZnO hybrid films.

are revealed by the magnified SEM images that indicate that the microcrystals in fact do not fully cover the ZnO film. To obtain the thickness of the as-prepared ZnO and Se films, cross-sectional identification is performed on a Si/SiO_2 substrate with a 200-nm oxide layer, as shown in Fig. 1e and 1f. The thicknesses of the Se layer and ZnO layer are ~ 2 μm and ~ 100 nm, respectively. This also shows good contact between the Se and ZnO film that will facilitate the carrier transport in the Se/ZnO heterojunction.

The elemental composition of the Se/ZnO hybrid film is analyzed by X-ray photoelectron spectroscopy (XPS), as shown in Fig. 1g. The spectrogram provides the detailed information about the Zn 2p, Se 3p, Se 3d, O 1s and C 1s peaks, which indicate the element feature of Se/ZnO hybrid film. The crystalline structure of the Se/ZnO hybrid film is further confirmed by X-ray diffraction (XRD) patterns. Figure 1h shows the XRD patterns of the Se, ZnO and Se/ZnO hybrid film, respectively. All peaks of the pure Se sample are well matched with selenium (JCPDS No. 65–1876) with lattice parameters of $a = b = 4.364$ Å and $c = 4.959$ Å. The sharp peak of the ZnO film located at 34.5° is assigned to the (002) plane of ZnO (JCPDS No. 36–1451) with lattice parameters of $a = \mathrm{b} = 3.250$ Å and $c = 5.207$ Å. The XRD pattern of the Se/ZnO hybrid film possesses peaks of both Se and ZnO films, which confirm the successful preparation of a hybrid Se/ZnO film.

The Se/ZnO hybrid structure fabricated on quartz substrate is then constructed into a device with indium electrodes, as schematically illustrated in Fig. 2a. It is worth noting that the incident light radiates the device from the back side, i.e. from ZnO to Se. This is mainly because front incident light from Se to ZnO will be blocked by the thick and opaque Se layer, leading to a lower optical photoresponse of ZnO. On the other hand, thin and transparent ZnO will ensure favorable light absorption of both Se and ZnO. Figure 2b shows a typical current–voltage (I–V) curve of the Se/ZnO PD in a semilogarithmic plot in the dark and upon 370-nm (0.85 mW cm^{-2}) UV light illumination. The dark current shows a symmetrical response for forward and reverse bias which is also obvious in linear coordinate, as shown in Fig. S2b, The linear dependence of current on voltage indicates good Ohmic contacts between the indium electrodes and Se/ZnO hybrid structure. The dark current at 5 V bias is ~ 0.6 nA, corresponding to a resistance of 8.3 TΩ at room temperature. The current increases by more than 2 orders of magnitude upon 370-nm UV light illumination. In addition to the dramatic current increase, the I-V curve also demonstrates an asymmetric feature for forward and reverse bias. Note that a relatively high current, reaching several nanoamperes exists at nominal zero bias, indicating that the Se/ZnO hybrid PD can operate without an external driving voltage, or as a self-powered PD that detects light without additional energy consumption. The self-powered effect of this device is mainly attributed to the photovoltaic effect from a p-n heterojunction by p-Se and n-ZnO, which will be discussed in detail in the following.

The responsivity of a device, defined as photocurrent per unit of incident power, is also important to evaluate the performance of a PD, which is usually calculated using the equation [28]:

$$R_\lambda = \frac{I_\lambda - I_d}{P_\lambda S} \tag{1}$$

where I_λ is the photocurrent, I_d is the dark current, P_λ is light power density and S is the photosensitive area, which

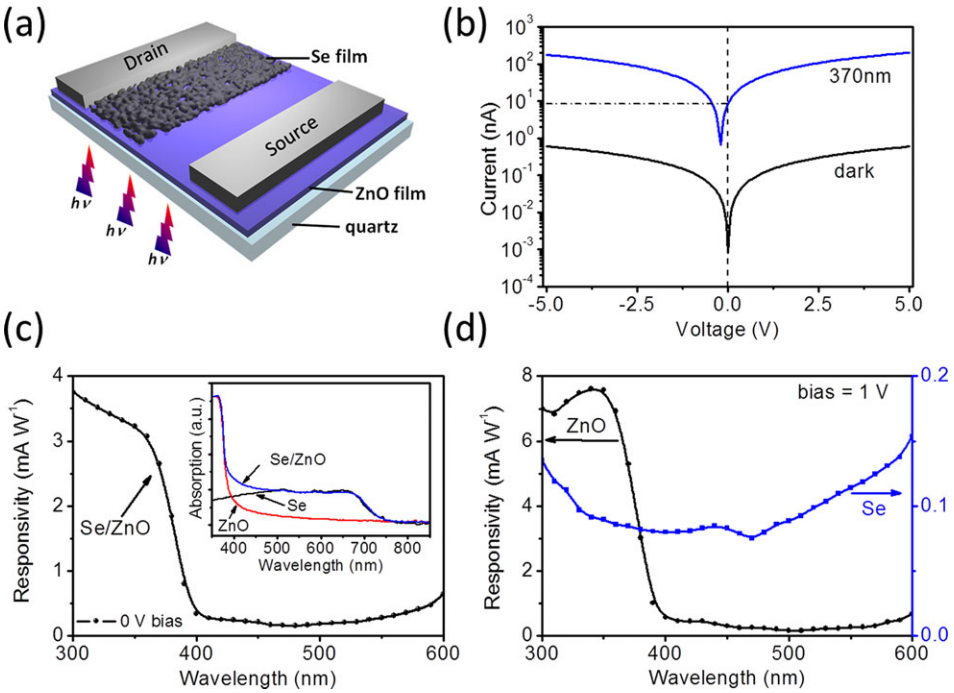

Figure 2 (a) Schematic diagram of Se/ZnO heterostructure UV PD. (b) *I–V* characteristics of the photodetector under dark and illumination with 370-nm UV light. (c) Spectral responsivity of the device under 0 V bias. Inset: UV-vis absorption spectra of Se, ZnO and Se/ZnO hybrid films. (d) Responsivity of pure ZnO and Se film under 1 V bias.

is 0.4 mm^2 for this Se/ZnO PD. The spectral responsivity at 0 V bias of the device is then calculated from 300 nm to 600 nm, as shown in Fig. 2c. The Fig. 2c inset shows the UV-vis absorption spectra of Se, ZnO and Se/ZnO hybrid films. The absorption spectrum of ZnO film shows intense change at ~400 nm and that of Se film shows intense change at ~750 nm. Interestingly, the absorption spectrum of the Se/ZnO hybrid film exhibits the optical properties of both Se and ZnO films. The absorption intensity first increases when wavelengths are shorter than ~750 nm, remains stable in the range 750–400 nm and then dramatically increases for wavelengths shorter than ~400 nm. The device shows good selectivity of UV light with a cut-off wavelength at ~400 nm, consistent with the spectral absorption spectrum in the inset. It can also be seen that the Se/ZnO PD exhibits a responsivity of 2.65 mA W^{-1} at zero bias under 370-nm UV radiation, comparable to a previously reported ZnO-based self-powered photodetector [20, 29]. At 5 V positive bias and 370-nm light illumination, the responsivity of this device reaches 60 mA W^{-1}, as shown in Fig. S2c. The UV-visible rejection ratio defined as $R_{300\ nm}/R_{400\ nm}$ is ~11 for our device at zero bias. The responsivity in the visible region of this device is mainly attributed to the low photoresponse of the Se layer and defects in the as-fabricated ZnO film that allows a small photoresponse in the visible region. This can be confirmed by Fig. 2d, which shows the spectral responsivity of the pure ZnO film and the Se film at 1 V bias. The ZnO film shows high and selective photoresponse in the UV region (<400 nm) while the Se film shows a broadband but weak photoresponse from the UV to the visible region.

The current–time (*I–t*) curve is measured with periodical on/off UV light illumination at zero bias, as shown in Fig. 3a. The device demonstrates high stability and repeatability under five cycles of switching on and off upon 0.85 mW cm^{-2} 370-nm UV irradiation. Moreover, the output current at zero bias rises to ~6 nA from nearly zero at the instant the UV light is switched on and decays to nearly zero at the instant the light is switched off. In the rise process, it is also clear that it is divided into two stages: a fast stage and a slow stage. The rise time of the combined two stages is several minutes in total. To identify the dark current at zero bias, a single period of the *I–t* curve on a semilogarithmic plot is given in Fig. 3b. The dark current is about 1 pA, while the photocurrent reaches ~10 nA, showing an on-off ratio of this device of about 10^4, which is at least one order of magnitude higher than previously reported self-powered devices [18, 20, 30, 31]. The linear dynamic range (LDR, quoted in dB) defined as:

$$\mathrm{LDR} = 20 \log \left(\frac{I_{ph}}{I_d} \right) \tag{2}$$

where I_{ph} is I_λ–I_d, is often adopted to describe the signal-to-noise ratio. The LDR of our device at zero bias is ~80 dB upon 370-nm 0.85 mW cm^{-2} UV light irradiation. The high LDR indicates a relatively large ratio of photocurrent to dark current and a high signal-to-noise ratio. Interestingly, the output current of this device at zero bias drops 3 orders of magnitude and rises nearly 4 orders of magnitude with off/on UV light, respectively, within 0.5 s (sample interval of two data points), indicating the fast response speed of the device. Due to the limitation of the sampling speed of the Keithley 4200-SCS semiconductor characterization system, the real response time of the device must be much shorter than 0.5 s as no point is recorded in the 0.5 s interval.

To better illustrate the time-resolved property and get more insight into the rise and decay time of the device, a

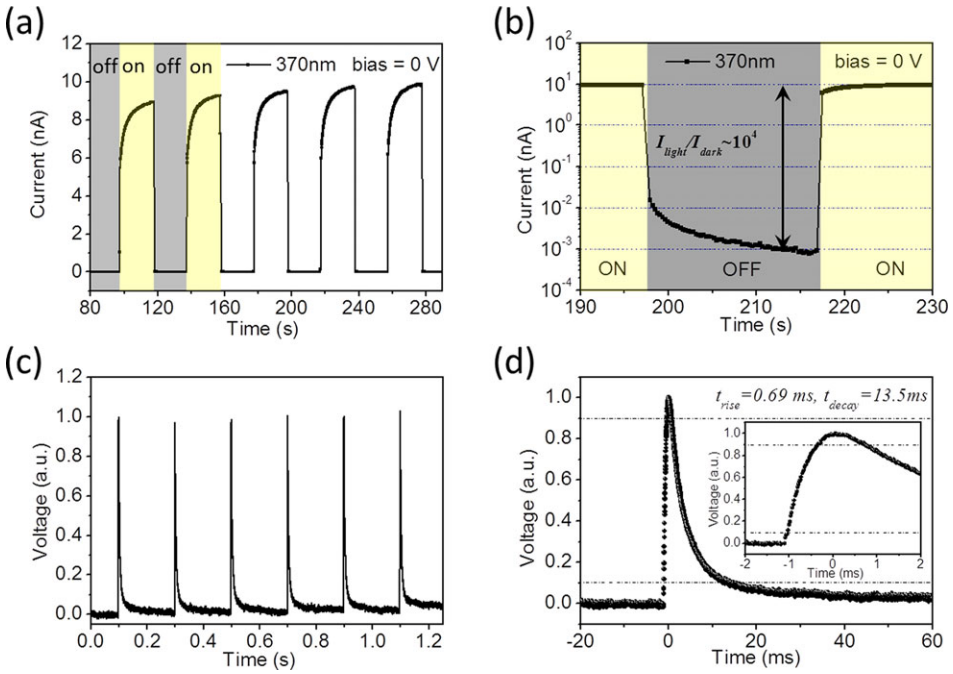

Figure 3 (a) *I–t* curve of Se/ZnO PD with periodical on/off switching upon 370-nm UV light illumination under 0 V bias. (b) Single period of the *I–t* curve on a semilogarithmic plot. (c) Pulse response of the Se/ZnO PD under 5-Hz 355-nm pulse laser radiation. (d) Single period of pulse response. Inset: rising edge of pulse response.

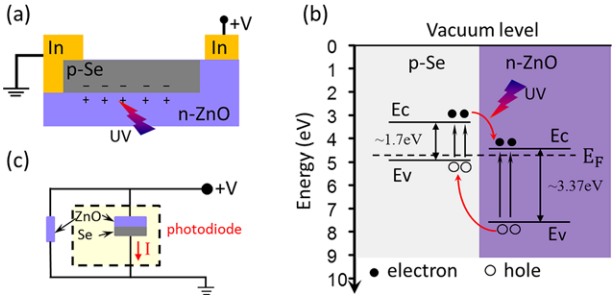

Figure 4 (a) Simplified schematic diagram of device structure. (b) Schematic illustration of energy levels of Se/ZnO heterojunction and charge-transfer process under UV light illumination. (c) Equivalent circuit of the Se/ZnO photodetector.

quick response measure system [32] is used with a 5-Hz 355-nm pulsed laser. Six cycles of the pulse response of the Se/ZnO PD are shown in Fig. 3c, which also confirms the stability and repeatability of the device. A single period of the pulse response in Fig. 3d shows the rise time of 0.69 ms (inset of Fig. 3d) and a decay time of 13.5 ms in Fig. 3d and inset. This is much quicker than that of a pure ZnO film with rise and decay times of 18 s and 56 s, respectively, as shown in Fig. S3. The rise and decay times are also of the same order as pure Se-based photodetector [24]. Because the rise and decay times are highly dependent on light intensity, the response time can be further shortened by increasing the light intensity [33].

To gain more insight into the mechanism of the self-powered Se/ZnO hybrid photodetector, the simplified structure of the device is illustrated in Fig. 4a. Because of the existence of interspace of Se microcrystal film as mentioned in Fig. 1d, the indium electrodes on top of Se film contact with not only Se film but also ZnO film, which lead to the device structure of Fig. 4a. This can also be proved by the linear dependence of dark current on voltage of Se/ZnO device, as shown in Fig. S2b. The dark current and photocurrent of Se films (Fig. S4) are lower than that of pure ZnO film (Fig. S3), indicating the higher resistance of the Se film. Therefore, the ZnO film is the primary carrier transport channel, leading to a linear characteristic of dark current for Se/ZnO device. On the other hand, the built-in electric field forms at the interface between p-Se and n-ZnO and the energy levels of Se and ZnO are displayed in Fig. 4b. In this diagram, the electron affinities (χ) of Se and ZnO are taken as 3.2 and 4.35 eV, respectively, and the bandgaps of Se and ZnO are 1.7 and 3.37 eV, respectively [34, 35]. Under UV-light illumination, photogenerated electrons and holes in the depletion layer are quickly separated by the built-in field, leading to the formation of photovoltages at both sides of the Se and ZnO. The equivalent circuit of the device is then illustrated in Fig. 4c. The device can be considered as the parallel connection between a ZnO photodetector and a Se/ZnO p-n heterojunction photodiode. As the hole mobility of Se is much lower than the electron mobility of ZnO, according to previous reports [8, 23], photogenerated electrons transfer faster from Se to ZnO than holes do from ZnO to Se. This implies that photogenerated electrons are collected earlier than photogenerated holes. This explains why the *I–t* curve in Fig. 3a consists of a faster process and a slower process corresponding to electron-transport processes in ZnO and hole-transport process in Se, respectively. When UV light is off at zero set bias, the photogenerated electron–hole pairs of Se recombine quickly, leading to rapid decay of the photovoltage to a relatively small value. Afterwards, the relatively long relaxation time is caused by an oxygen reabsorption process of ZnO, which is responsible for the

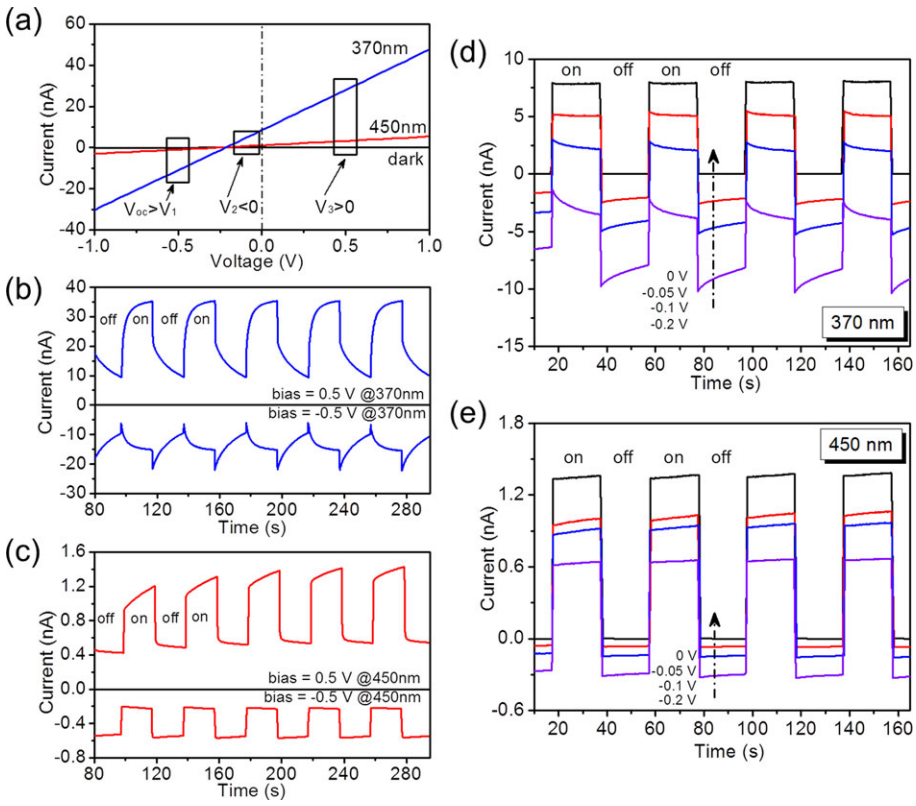

Figure 5 (a) *I–V* curves of Se/ZnO hybrid under dark and 370 nm (0.85 mW cm^{-2}) and 450 nm (1.003 mW cm^{-2}) light illumination. (b,c) *I–t* curves under 370-nm and 450-nm light illumination at 0.5 V and –0.5 V bias. (d,e) *I–t* curves under 370-nm and 450-nm light illumination at 0 V bias and small negative bias of –0.05 V, –0.1 V and –0.2 V.

slow degradation of the dark current, as shown in Fig. 3b. In addition to working at zero bias, the theoretical equivalent circuit of parallel connection promises the device will work at different biases to achieve multifunction operation.

The binary response characteristic of the device is further studied at different bias voltages and wavelengths. Figure 5a shows the *I–V* curves of the Se/ZnO device under dark conditions, 370-nm (0.85 mW cm^{-2}) UV light and 450-nm (1.003 mW cm^{-2}) visible light. Different bias (–0.5 V, –0.2 V, –0.1 V, –0.05 V, 0 V and 0.5 V) are adopted in our study according to the open-circuit voltage (V_{oc}) of the device, as seen in Fig. 5a. Figure 5b and 5c show the *I–V* curves at 0.5 V and –0.5 V under 370-nm and 450-nm light illumination, respectively. Under 0.5 V and –0.5 V biases, the *I–t* curves under both 370-nm UV light and 450-nm visible illuminations show an asymmetrical shape in that the photocurrent is higher under positive bias than under negative bias. This is mainly caused by the photogenerated current flowing from ZnO to Se. When an external voltage is applied, the total current collected is the sum of the current on ZnO and on the Se/ZnO photodiode, as depicted in Fig. 4c. As the current directions of ZnO and Se/ZnO photodiode are the same under positive bias, the total current is enhanced. While at a negative bias of –0.5 V, which is opposite to the direction of the photocurrent generated by photovoltaic effect in the Se/ZnO photodiode, the total current is decreased. In addition, the sudden rise is observed when UV light is turned off at –0.5 V bias in Fig. 5b, which is also the evidence for different directions of current flow on ZnO and photogenerated current on Se/ZnO photodiode. Under 450-nm visible light illumination at –0.5 V bias, the photocurrent decreases when the light is switched on and rises when the light is switched off. This is due to the photogenerated current arising from the photovoltaic effect on the Se/ZnO diode and the broadband photoresponse of Se. When the bias is set as –0.05 V and –0.1 V ($V_{oc}<V<0$), the *I–t* curves under both 370-nm UV light and 450-nm visible light demonstrate a binary response that the output current alternates between negative and positive when the light is switched on and off as shown in Fig. 5d and 5e. However, at –0.2 V bias, the *I–t* curve under 370-nm irradiation demonstrates a nonbinary response property, which is different from that under 450-nm light irradiation. This is mainly because the absolute value of V_{oc} under 370-nm light irradiation is smaller than that under 450-nm light irradiation. The binary response of the device can also be explained by the equivalent circuit depicted in Fig. 4c. In the dark, the small negative bias can produce a negative current in the circuit, while the photogenerated forward current from the Se/ZnO heterojunction is dominant upon light illumination and results in the current changing from negative to positive. This phenomenon provide an additional pathway to remove the negative effect of the noise signal and might fulfill the demand of weak-signal detection [36].

4. Conclusions and outlook

In summary, we have developed a high-performance UV photodetector based on a Se/ZnO p-n heterojunction. The built-in field at the interface of Se and ZnO allows the device to operate without an external energy supply. The

speed of the ZnO UV PD is greatly improved with a rise time of 0.69 ms and a decay time of 13.5 ms, which are much quicker than those of pure ZnO film PDs. The device also exhibits a high on/off ratio of 10^4 and a responsivity of 2.65 mA W^{-1} using a low power density UV light source (0.85 mW cm^{-2}, 370 nm) without any electrical power source. More interestingly, at a small reverse bias, the device achieves a binary response of positive and negative output current using an on/off light source. The novel phenomenon is explained by the parallel connection of ZnO and the Se/ZnO hybrid structure and might be potentially useful for binary light communication and relative applications with weak-signal detection. The results reported in this paper provide a facile route to fabricate ZnO-based p-n junction UV photodetectors with high sensitivity, high signal-to-noise ratio, high spectral selectivity, high speed, and high stability and thus may lay a solid ground for the future applications of this kind of high-performance multifunctional photodetector.

Supporting Information

Additional supporting information may be found in the online version of this article at the publisher's website.

Acknowledgements. This work was supported by the National Natural Science Foundation of China (Grant Nos. 51471051, 61505033 and 11674061), the National Postdoctoral Science Foundation of China (2015M580294), the Science and Technology Commission of Shanghai Municipality (15520720700), the Shanghai Shu Guang Project (12SG01), and the Programs for Professor of Special Appointment (Eastern Scholar) at Shanghai Institutions of Higher Learning. Part of this work was carried out in the Fudan Nano-fab Laboratory.

Received: 28 September 2016, **Revised:** 28 November 2016, **Accepted:** 29 November 2016

Published online: 21 December 2016

Key words: binary response, Se/ZnO heterojunction, UV photodetector, high on/off ratio, fast speed.

References

[1] H. Y. Chen, H. Liu, Z. M. Zhang, K. Hu, and X. S. Fang, Adv. Mater. **28**, 403 (2016).
[2] L. W. Sang, M. Y. Liao, and M. Sumiya, Sensors (Basel) **13**, 10482 (2013).
[3] Z. Jin, Q. Zhou, Y. Chen, P. Mao, H. Li, H. Liu, J. Wang, and Y. Li, Adv. Mater. **28**, 3697 (2016).
[4] X. Liu, L. L. Gu, Q. P. Zhang, J. Y. Wu, Y. Z. Long, and Z. Y. Fan, Nature Commun. **5**, 4007 (2016).
[5] L. E. Greene, M. Law, J. Goldberger, F. Kim, J. C. Johnson, Y. Zhang, R. J. Saykally, and P. Yang, Angew. Chem. **115**, 3139 (2003).
[6] L. Peng, L. F. Hu, and X. S. Fang, Adv. Mater. **25**, 5321 (2013).
[7] Z. Jin and J. Wang, J. Mater. Chem. C **2**, 1966 (2014).
[8] Y. Jin, J. Wang, B. Sun, J. C. Blakesley, and N. C. Greenham, Nano Lett. **8**, 1649 (2008).
[9] Z. Jin, L. Gao, and Q. Zhou, J. Wang, Sci. Rep. **4**, 4268 (2014).
[10] A. Bera and D. Basak, Appl. Phys. Lett. **93**, 053102 (2008).
[11] C. H. Liu, Y. C. Chang, T. B. Norris, and Z. H. Zhong, Nature Nanotechnol. **9**, 273 (2014).
[12] M. R. Hasan, T. Xie, S. C. Barron, G. Liu, N. V. Nguyen, A. Motayed, M. V. Rao, and R. Debnath, APL Mater. **3**, 106101 (2015).
[13] N. Nasiri, R. Bo, F. Wang, L. Fu, and A. Tricoli, Adv. Mater. **27**, 4336 (2015).
[14] N. Nasiri, R. Bo, H. Chen, T.P. White, L. Fu, and A. Tricoli, Adv. Opt. Mater. **4**, 1787 (2016).
[15] N. Nasiri, R. Bo, T. F. Hung, V. A. L. Roy, L. Fu, and A. Tricoli, Adv. Funct. Mater. **26**, 7359 (2016).
[16] H. Y. Chen, K. W. Liu, L. F. Hu, A. A. Al-Ghamdi, and X. S. Fang, Mater. Today **18**, 493 (2015).
[17] H. Shen, C. Shan, B. Li, B. Xuan, and D. Shen, Appl. Phys. Lett. **103**, 232112 (2013).
[18] W. Jin, Y. Ye, L. Gan, B. Yu, P. Wu, Y. Dai, H. Meng, X. Guo, and L. Dai, J. Mater. Chem. **22**, 2863 (2012).
[19] L. Peng, L. F. Hu, and X. S. Fang, Adv. Funct. Mater. **24**, 2591 (2014).
[20] S. M. Hatch, J. Briscoe, and S. Dunn, Adv. Mater. **25**, 867 (2013).
[21] K. Murphy, B. Wunderlich, and B. Wunderlich, J. Phys. Chem. **86**, 2827 (1982).
[22] Z. M. Liao, C. Hou, Q. Zhao, L. P. Liu, and D. P. Yu, Appl. Phys. Lett. **95**, 093104 (2009).
[23] T. Masuzawa, I. Saito, T. Yamada, M. Onishi, H. Yamaguchi, Y. Suzuki, K. Oonuki, N. Kato, S. Ogawa,and Y. Takakuwa, Sensors **13**, 13744 (2013).
[24] L. B. Luo, X. B. Yang, F. X. Liang, J. S. Jie, Q. Li, Z. F. Zhu, C. Y. Wu, Y. Q. Yu, and L. Wang, Cryst. Eng. Comm. **14**, 1942 (2012).
[25] P. Liu, Y. Ma, W. Cai, Z. Wang, J. Wang, L. Qi, and D. Chen, Nanotechnology **18**, 205704 (2007).
[26] K. Hu, H. Y. Chen, M. M. Jiang, F. Teng, L. X. Zheng, and X. S. Fang, Adv. Funct. Mater. **26**, 6641 (2016).
[27] W. Kai, C. Feng, G. Belev, S. Kasap, and K. S. Karim, Appl. Phys. Lett. **95**, 013505 (2009).
[28] H. Liu, Z. M. Zhang, L. F. Hu, N. Gao, L. W. Sang, M. Y. Liao, R. Z. Ma, F. F. Xu, and X. S. Fang, Adv. Opt. Mater. **2**, 771 (2014).
[29] P. N. Ni, C. X. Shan, S. P. Wang, X. Y. Liu, and D. Z. Shen, J. Mater. Chem. C **1**, 4445 (2013).
[30] L. Mandal, N. S. Chaudhari, and S. Ogale, ACS Appl. Mater. Interface. **5**, 9141 (2013).
[31] O. Game, U. Singh, T. Kumari, A. Banpurkar, and S. Ogale, Nanoscale **6**, 503 (2014).
[32] M. M. Fan, K. W. Liu, X. Chen, Z. Z. Zhang, B. H. Li, H. F. Zhao, and D. Z. Shen, J. Mater. Chem. C **3**, 313 (2015).
[33] Y. Jiang, W.J. Zhang, J. S. Jie, X. M. Meng, X. Fan, and S. T. Lee, Adv. Funct. Mater. **17**, 1795 (2007).
[34] S. K. Joshi and C. D. Lokhande, Appl. Surf. Sci. **252**, 8539 (2006).
[35] I. S. Jeong, J. H. Kim, and S. Im, Appl. Phys. Lett. **83**, 2946 (2003).
[36] Q. Hong, Y. Cao, J. Xu, H. Lu, J. He, and J. L. Sun, ACS Appl. Mater. Interface. **6**, 20887 (2014).